

Jefferson Lab PAC 34 Proposal

**Precise Measurement of π^+/π^- Ratios in Semi-inclusive Deep
Inelastic Scattering Part II: Unraveling the Flavor Dependence of
the EMC Effect**

December 16, 2008

J. Arrington, R. Dupré, D. Geesaman, K. Hafidi (spokesperson), R. J. Holt, D. H. Potterveld,
P. E. Reimer, P. Solvignon

Argonne National Laboratory, Argonne, IL

W. Chen, H. Gao, X. Qian, Y. Qiang, Q. Ye

Duke University, Durham, NC

P. Markowitz

Florida International University, Miami, FL

C. E. Keppel

Hampton University, Hampton, VA

G. Niculescu, I. Niculescu

James Madison University, Harrisonburg, VA

P. Bosted, R. Ent, H. Fenker, D. Gaskell (spokesperson), T. Horn, M. K. Jones, D. Mack,
G. Smith, S. Wood

Jefferson Lab, Newport News, VA

J. Dunne, D. Dutta (spokesperson¹), E. Leggett, A. Narayan, L. Ndukum, Nuruzzaman, A. Subedi
Mississippi State University, Mississippi State, MS

A. Daniel

Ohio University, Athens, OH

E. Beise

University of Maryland, College Park, MD

G. Huber

University of Regina, Regina, SK, Canada

H. Baghdasaryan, D. Day, N. Kalantarians, O. Rondon

University of Virginia, Charlottesville, VA

I. C. Cloët

¹ Contact person, d.dutta@msstate.edu

University of Washington, Seattle, WA

F. .R. Wesselman

Xavier University of Louisiana, New Orleans, LA

A. Asaturyan, A. Mkrtchyan, H. Mkrtchyan, V. Tadevosyan

Yerevan Physics Institute, Yerevan, Armenia

I. CONTRIBUTION TO THE HALL C 12 GEV UPGRADE

The co-spokespersons for this experiment plan to contribute to the implementation of the Hall C upgrade for 12 GeV in both manpower and materials.

Dipangkar Dutta will help design and commission the collimators and sieve slits for the SHMS spectrometer. He is seeking funding to build a GEM based forward tracker which in combination with the slits and collimators will be used to understand and model the magnetic transport of the spectrometer. He is also seeking funding to build an aerogel Čerenkov counter for the SHMS (not part of baseline equipment). His group will also contribute manpower towards the upgrade and commissioning of the SHMS.

David Gaskell will support the SHMS construction and detector assembly and is responsible for ensuring functionality of the Hall C Møller and Compton polarimeters at 12 GeV. In addition, he will devote time to updating and maintaining the Hall C simulation package SIMC. This will entail, not only incorporating the SHMS into the existing simulation, but helping with spectrometer optics calculations.

Kawtar Hafidi and the Argonne group has been contributing towards the initial optics design of the SHMS. They will also perform optics commissioning and verification of the SHMS.

II. ABSTRACT

We propose to measure precision ratios of charged pion electroproduction in Semi-Inclusive Deep Inelastic Scattering from deuterium and gold targets. This experiment is Part II of a program of two experiments. In Part I, data from the deuterium target alone will be used to test the validity of charge symmetry in the valence quark distributions. In this experiment, gold and deuterium data will be combined to test the flavor dependence of the EMC effect in the valence region. The two experiments are proposed together due to the similar technique, i.e. precision measurements of charged pion ratios, and overlap in kinematics.

This experiment will use the SHMS and HMS in Hall C to measure electrons and charged pions in coincidence. In this case, the SHMS will be used as the electron arm, and the HMS as the hadron arm. The experiment will measure semi-inclusive production of charged pions over a range of $x=0.2$ to 0.6 , where valence quarks dominate and at fixed $z = 0.5$. In addition, extensive measurements covering a range of ν and z will be taken at $x = 0.3$, where the EMC effect is small, to fully map out any differences in hadron attenuation effects between π^+ and π^- production.

We will form the double ratio of yields, $R_{Au/D}^{\pi^+/\pi^-} = [Y_{Au}(\pi^+)/Y_{Au}(\pi^-)]/[Y_D(\pi^+)/Y_D(\pi^-)]$, and the difference ratio $R_{Au/D}(\pi^+ - \pi^-) = [Y_{Au}(\pi^+) - Y_{Au}(\pi^-)]/[Y_D(\pi^+) - Y_D(\pi^-)]$ in order to search for evidence of flavor dependence of the EMC effect. Our simulations show that these two variables are most sensitive to flavor dependence of the EMC effect. Evidence of a flavor dependence in the EMC effect will place strict constraints on models of the EMC effect and give us new information regarding the effect of the nuclear environment on quarks. This experiment will also have impact on calculations or experiments that rely on knowledge of nuclear parton distributions at large x .

This experiment, run alone, requires 24 days to complete in Hall C assuming a maximum of $50 \mu\text{A}$ beam current and a beam energy of 11 GeV. The majority of the deuterium data needed in this proposal is taken at common kinematics with Part I; if Part I and Part II run together, the total time needed is 34 days.

III. INTRODUCTION

One of the longstanding goals of nuclear physics is to understand how nuclei can be described in terms of gluons exchanged by colored quarks and gluons of the fundamental theory of the strong force – Quantum Chromo Dynamics (QCD). Revealing QCD as the ultimate source of the strong interaction requires exploring the true nature of color confinement. Nuclei provide an excellent testing ground for QCD because they are a stable system made up of quarks and gluons bound together by the strong force. However, the quarks and gluons in nuclei are hidden and they seem to be composed of nucleons bound together by exchanging mesons. Consequently, over the last several decades a significant amount of effort has been invested in the study of nuclear structure at small distances with the aim of mapping out the quark distributions inside the nucleus. One of the most surprising and influential results from these studies, was the discovery in 1983 of the so called “EMC effect.”

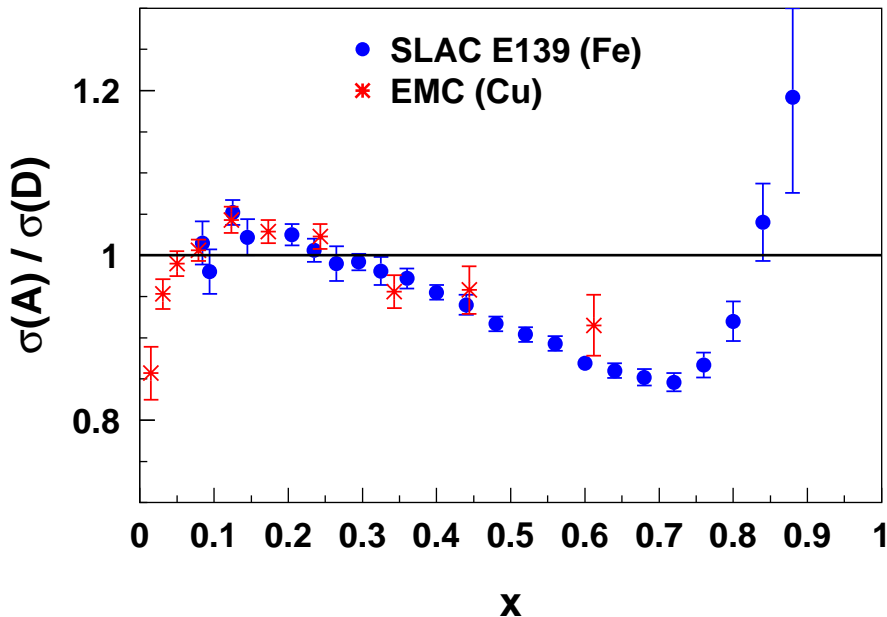


FIG. 1: Cross section ratios from copper and iron to deuterium from the EMC [11] and SLAC E139 [4] experiments.

The depletion of the structure function in a nucleus as compared to that in a free nucleon (see Fig. 1) was discovered by the EMC collaboration [1] and has been dubbed as the “EMC effect.” These modifications in the nuclear structure function demonstrated that nuclei cannot be described merely as a collection of nucleons, thereby injecting the subject of quarks into nuclear physics. Since its original observation by the EMC collaboration, the modification of structure functions in nuclei has created an industry of theoretical and experimental effort (see [2] and [3] for an overview). For example, in the valence regime, the A and x

dependence of the depletion in the nuclear structure function has been precisely mapped out using inclusive deep inelastic scattering (DIS) studies by the SLAC E139 experiment [4]. More recently data from HERMES [5] and JLab [6] have contributed new information on the EMC Effect in the few body regime. On the theoretical side, a multitude of approaches (also reviewed extensively in [2] and [3]), ranging from nuclear binding and convolution models, to dynamical quark rescaling, and more recently including a quark-meson coupling inspired approach [7] are all able to describe the EMC effect quite adequately in the valence quark (high x) regime. However, the specific origin of the observed modifications have not yet been unambiguously identified. The inclusive nature of the previous measurements does not provide sufficient insight into the QCD mechanism for the depletion of the DIS structure functions. All of the measurements at large x are basically, more complete and higher precision, measurements of the same observable, i.e., σ_A/σ_D . The only additional constraint to date comes from measurements of the A -dependence of the sea distribution in Drell-Yan reactions [10]. Therefore, all we can say for certain is that the EMC effect requires the presence of some non-nucleonic degrees of freedom in nuclei and there is a great need for new experimental techniques that would unravel the EMC effect and thereby provide a better handle on understanding the QCD dynamics of multi-nucleon systems at small distances.

One such experimental technique holding a lot of promise is the semi-inclusive DIS reaction. Semi-inclusive DIS can be used as a “flavor tag” (see Fig. 2) to look for signatures of differences in the EMC effect in the up and down quark distributions in asymmetric nuclei (e.g. gold). It has been used successfully, most notably by the HERMES collaboration [12], to deconvolute the relative contributions of up, down, and sea quarks to the spin of the nucleon. However, one can just as easily employ the power of this technique to probe the unpolarized degrees of freedom rather than polarized parton distributions. Moreover, the two well understood, high resolution magnetic spectrometers in the upgraded Hall-C will allow measurements with precision unattainable by large acceptance devices, and thus lead to precision tomography of the EMC effect.

IV. SCIENTIFIC MOTIVATION: FLAVOR DEPENDENCE OF THE EMC EFFECT

The flavor dependence of the EMC effect is one of the most promising new avenues that will become accessible for precision studies at the upgraded JLab. It has the most potential to distinguish between the plethora of models that can describe the EMC effect. In the simplest picture, we can consider the nuclear parton distribution functions (PDFs) to be just the nucleon PDFs smeared by the Fermi motion of the nucleons. In this picture it is natural to assume that the modifications to the valance quark distributions in the nucleus will be the same for up and down quarks. However, there is no experimental evidence

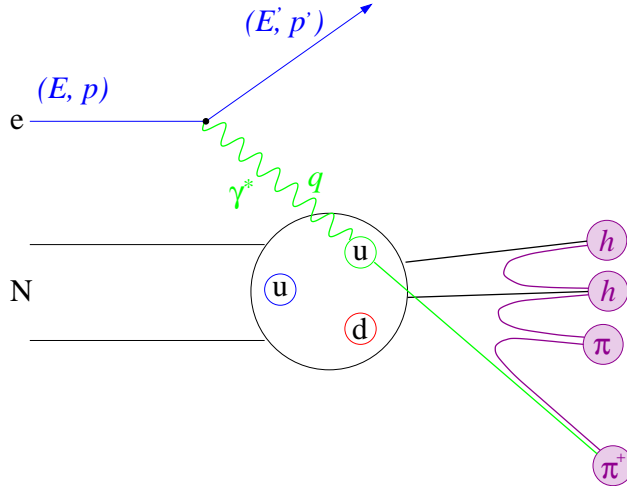


FIG. 2: Diagram of semi-inclusive pion production from the nucleon. In this picture, the observed hadron (in this case the π^+) serves as a “tag” of the flavor of the struck (up) quark.

that this assumption is true. In fact a recent calculation [13] in the quark-meson coupling inspired approach [7], suggests that there might be a large flavor dependence in asymmetric nuclei ($N > Z$). Fig. 3 shows a calculation of the EMC effect in gold (an asymmetric nucleus with $N/Z = 1.5$) using the model of Ref. [7]. In this case, the isospin dependent part of the nuclear potential generates a difference in the modification of the up and down quark distributions. Such a flavor dependence would be a clear and unambiguous signature of actual medium modification of the quark distribution functions. Moreover, experimental observation of flavor dependence of the EMC effect would place stringent constraints on models of the EMC effect. For example simple convolution models and flavor independent quark rescaling models would be ruled out by the observation of any flavor dependence.

In this experiment we propose to study the flavor dependence of the EMC effect at large x using a new observable, as suggested in Ref. [9]². We will measure the ratio of charged pion electroproduction in semi-inclusive DIS from deuterium and gold targets. The new observables proposed here are the super-ratio of yields, $\frac{\pi^+}{\pi^-}$, from gold to deuterium and the ratio of the difference in yields ($\pi^+ - \pi^-$) from gold to deuterium. We will show in the next few sections that these observables, in asymmetric nuclei (i.e. $N > Z$), are very sensitive to any flavor dependence in modifications to the structure functions inside a nucleus. Thus, by performing a precision measurement of these observables we hope to expose any flavor dependence in the EMC effect and thereby reveal the details of the quark dynamics in nuclei which lead to the modification of the nuclear structure functions. The overall motivation for

² In Ref. [9], semi-inclusive processes were proposed as a way to measure the nuclear sea quark content. Pion electroproduction, not surprisingly, is not terribly sensitive to sea quarks at large x .

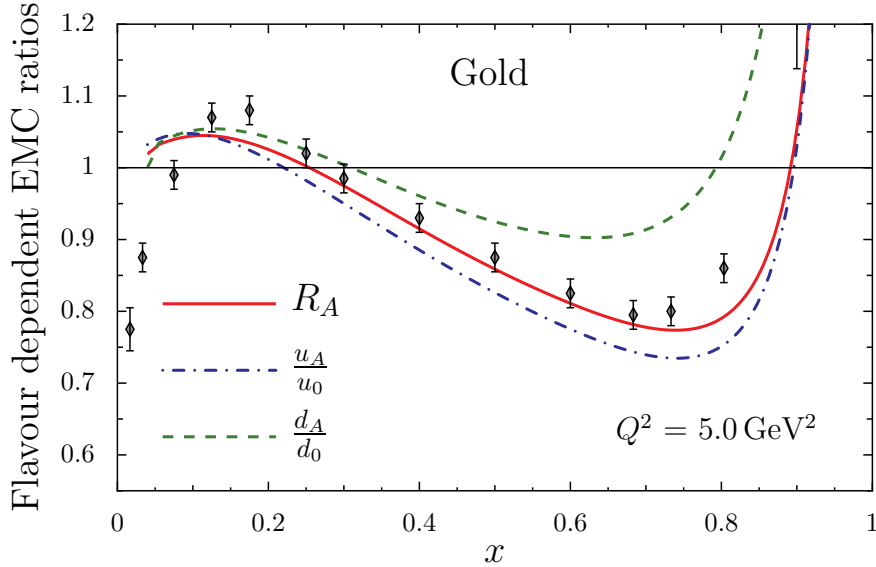


FIG. 3: Calculation of the EMC Effect in gold from [13]. Here, “gold” actually refers to a calculation for nuclear matter, but assuming the same N/Z as gold. In this model, nuclear quark distributions are modified via interactions with vector and scalar fields in the nucleus. The solid red curve shows the overall modification of the nuclear structure function, F_2 . The isospin dependence of the interaction generates a different degree of modification for the up and down quark distributions (shown by the green and blue curves respectively). Data points are from [8].

our proposal is to provide insight into the nature of color confinement and the role of quarks in nuclei.

V. FORMALISM

In general, the cross section for the semi-inclusive production of a charged pion can be written,

$$\frac{d\sigma}{dx dQ^2 dz} = \frac{\sum_f e_f^2 q_f(x, Q^2) D_f^h(z, Q^2)}{\sum_f e_f^2 q_f(x, Q^2)} \frac{d\sigma}{dx dQ^2}, \quad (1)$$

where $\frac{d\sigma}{dx dQ^2}$ is the inclusive electron scattering cross section, $q_f(x, Q^2)$ is the distribution function for a quark of flavor f and charge e_f and $D_f^h(z, Q^2)$ is the fragmentation function describing the probability for a quark of flavor f to be found in a hadron of species h carrying a fraction $z = E_h/\nu$ of the energy of the struck quark. Note that we have ignored the azimuthal angle ϕ and transverse momentum p_t of the outgoing hadron in this expression. In this experiment we will be detecting hadrons along the direction of the 3 momentum transfer q (i.e. in parallel kinematics) so that $p_t \approx 0$.

A. Nuclear Parton Distribution Functions

It is convenient at this point to define the nuclear parton distribution functions. For a nucleus of Z protons and N neutrons we define the nuclear PDF (per nucleon) for up and down quarks as,

$$\begin{aligned} u_A &= \frac{Z\tilde{u}_p + N\tilde{u}_n}{A} \\ d_A &= \frac{Z\tilde{d}_p + N\tilde{d}_n}{A}, \end{aligned} \quad (2)$$

where $(\tilde{u}_p, \tilde{u}_n)$ and $(\tilde{d}_p, \tilde{d}_n)$ are the up and down quark distributions in the protons and neutrons of the nucleus and the tilde signifies that the quark distribution may be modified in the nuclear medium. Assuming isospin symmetry between the proton and neutron such that

$$u(x) = u_p(x) = d_n(x) \quad (3)$$

$$d(x) = d_p(x) = u_n(x), \quad (4)$$

the above can be expressed,

$$\begin{aligned} u_A &= \frac{Z\tilde{u}_p + N\tilde{d}_p}{A} \\ d_A &= \frac{Z\tilde{d}_p + N\tilde{u}_p}{A}. \end{aligned} \quad (5)$$

Similar expressions apply for the antiquarks. In the absence of medium modifications to the PDFs the above expression becomes,

$$\begin{aligned} u_0 &= \frac{Zu_p + Nd_p}{A} \\ d_0 &= \frac{Zd_p + Nu_p}{A}. \end{aligned} \quad (6)$$

B. Flavor Dependence of the EMC Effect

The semi-inclusive yield of charged pions from a nucleus of Z protons and N neutrons can be written,

$$\begin{aligned} N_A^{\pi^+}/A &= \frac{4}{9}u_A(x)D_A^+(z) + \frac{1}{9}d_A(x)D_A^-(z) + \frac{1}{9}\bar{d}_A(x)D_A^+(z) + \frac{4}{9}\bar{u}_A(x)D_A^-(z) \\ N_A^{\pi^-}/A &= \frac{4}{9}u_A(x)D_A^-(z) + \frac{1}{9}d_A(x)D_A^+(z) + \frac{1}{9}\bar{d}_A(x)D_A^-(z) + \frac{4}{9}\bar{u}_A(x)D_A^+(z), \end{aligned} \quad (7)$$

where we have used the nuclear PDFs defined in the previous section and the subscript A on the fragmentation functions refers to the fact that they may also be modified in the

nuclear environment. We have used the favored and unfavored fragmentation functions, $D^+ = D_u^{\pi^+} = D_d^{\pi^+} = D_d^{\pi^-} = D_u^{\pi^-}$ and $D^- = D_d^{\pi^+} = D_u^{\pi^+} = D_u^{\pi^-} = D_d^{\pi^-}$. Note that we have also ignored strange quark degrees of freedom as well as any Q^2 dependence in the PDFs and fragmentation functions for simplicity.

To investigate the flavor dependence of the EMC effect, we can look at a number of quantities. First, we can look at the sum of π^+ and π^- yields in a nucleus compared to that from deuterium. This can be expressed:

$$\frac{Y(\pi^+ + \pi^-)_A}{Y(\pi^+ + \pi^-)_D} = \frac{4[u_A(x) + \bar{u}_A(x)] + [d_A(x) + \bar{d}_A(x)]}{5[u(x) + d(x) + \bar{u}(x) + \bar{d}(x)]} \times \frac{D_A^+(z) + D_A^-(z)}{D^+(z) + D^-(z)}, \quad (8)$$

where we have used nucleon PDFs to describe the parton distributions in deuterium, assuming no medium modifications for $A = 2$. This expression, in the absence of medium modifications to the fragmentation functions, is simply another way of expressing the usual ratio of inclusive structure functions, so not useful for extracting new information regarding the EMC effect. This expression, however, will prove useful for other purposes as will be described later.

Similarly, one can also extract the ratio of the difference of yields in charged pion production:

$$\frac{Y(\pi^+ - \pi^-)_A}{Y(\pi^+ - \pi^-)_D} = \frac{4[u_A(x) - \bar{u}_A(x)] - [d_A(x) - \bar{d}_A(x)]}{3[u_v(x) + d_v(x)]} \times \frac{D_A^+(z) - D_A^-(z)}{D^+(z) - D^-(z)}. \quad (9)$$

Here we have made the assumption $u(x) = u_v(x) + \bar{u}(x)$. One must know in this case to what degree fragmentation functions are modified in the nuclear medium to extract meaningful information about modifications to the parton distributions in nuclei.

Finally, we can examine the π^+/π^- ratio. This has the advantage that, to the extent that hadron attenuation effects are the same for both π^+ and π^- production, these effects cancel in the charge ratio and no explicit correction is needed.

$$Y_A\left(\frac{\pi^+}{\pi^-}\right) = \frac{[4u_A(x) + \bar{d}_A(x)] D_A^+(z) + [d_A(x) + 4\bar{u}_A(x)] D_A^-(z)}{[4u_A(x) + \bar{d}_A(x)] D_A^-(z) + [d_A(x) + 4\bar{u}_A(x)] D_A^+(z)}, \quad (10)$$

and

$$Y_A\left(\frac{\pi^+}{\pi^-}\right)/Y_D\left(\frac{\pi^+}{\pi^-}\right) = \frac{[4u_A(x) + \bar{d}_A(x)] D_A^+(z) + [d_A(x) + 4\bar{u}_A(x)] D_A^-(z)}{[4u_A(x) + \bar{d}_A(x)] D_A^-(z) + [d_A(x) + 4\bar{u}_A(x)] D_A^+(z)} \times \frac{[4u_D(x) + \bar{d}_D(x)] D^-(z) + [d_D(x) + 4\bar{u}_D(x)] D^+(z)}{[4u_D(x) + \bar{d}_D(x)] D^+(z) + [d_D(x) + 4\bar{u}_D(x)] D^-(z)} \quad (11)$$

The above expression is useful in that the experimental advantages in performing simple ratios of charged pion yields allows one to make a potentially very precise measurement of this quantity, increasing one's sensitivity to a possible flavor dependence of the EMC effect.

In Fig. 4 we show our sensitivity to a potential flavor dependence of the EMC effect using the last two approaches mentioned above, as described in Eqns. 9 and 11. The calculations shown in Fig. 4 are performed using nuclear PDFs obtained from a global analysis of experimental structure function data and Drell-Yan cross-section ratios by Hirai, Kumano and Nagai [14]. Since they are based on measured nuclear structure functions, the nuclear PDFs include the EMC effect, but they assume that the modifications of the up and down quark distributions inside the nucleus are exactly the same. In addition to the nuclear PDFs we use a parameterization of the sum of favored and unfavored fragmentation functions from Binnewies *et al* [15] and the ratio D^-/D^+ from a parameterization of HERMES data [16]. This parameterization has been shown to agree well with Hall C semi-inclusive data up to $z \approx 0.7$ [18].

In order to investigate the sensitivity of the flavor dependence of the EMC effect, we calculated two hybrid nuclear PDFs such that all of the EMC effect is given by modification of only the up quark and down quark distributions respectively. For the case where the EMC effect is due to modification of the up quark distribution only, we used;

$$u_A(x) = u_A^{\text{nucl}}(x) + \frac{1}{4} \left[d_A^{\text{nucl}}(x) - d_0(x) \right]$$

and

$$d_A(x) = d_0(x)$$

and for the case where the EMC effect is due to the modifications of the down quark distribution only, we used;

$$u_A(x) = u_0(x)$$

and

$$d_A(x) = d_A^{\text{nucl}}(x) + 4 \left[u_A^{\text{nucl}}(x) - u_0(x) \right],$$

where $u_A^{\text{nucl}}(x)$ and $d_A^{\text{nucl}}(x)$ are the nuclear PDFs from Ref. [14] which include the EMC effect but assumes the EMC effect is flavor independent, and $u_0(x) = [Zu(x) + Nd(x)]/A$ and $d_0(x) = [Zd(x) + Nu(x)]/A$ are the nuclear PDFs for a nucleus with Z protons and N neutrons, constructed from the nucleon PDFs $u(x)$ and $d(x)$ (we used MRST01-LO [17]). Note that $u_0(x)$ and $d_0(x)$ do not include any EMC effect. This formalism ensures that the nuclear structure function,

$$F_2^A = xA \left(\frac{4}{9} [u_A(x) + \bar{u}_A(x)] + \frac{1}{9} [d_A(x) + \bar{d}_A(x)] \right),$$

remains unchanged whether one uses the nuclear PDFs of Ref. [14] or the two hybrid nuclear PDFs described above.

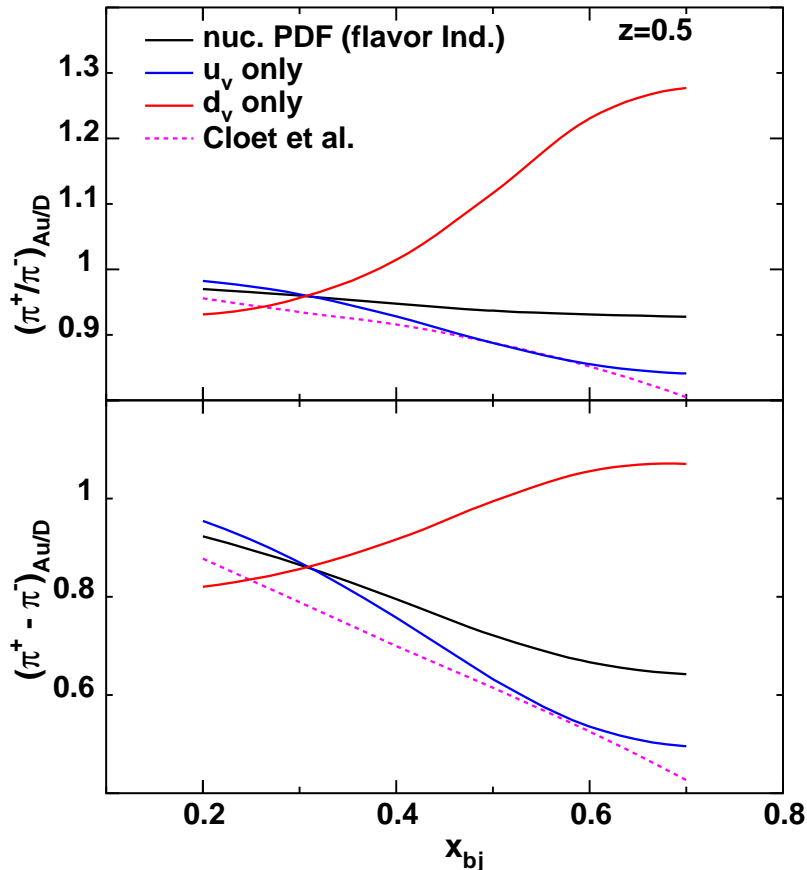


FIG. 4: Calculations of the quantities described in Eqs. 9, and 11. In these calculations we show each observable under the assumption that 1) the EMC effect is the same for up and down quarks (black), 2) the EMC effect is carried entirely by the up valence quark (blue) and 3) the EMC effect is carried entirely by the down valence quark (red). We also show the calculation of [13] which yields effects similar to those predicted by the “all up” scenario.

Hadron attenuation is an important issue for any experiment that proposes to use semi-inclusive DIS to study the EMC effect and will be discussed in detail in the next section. In the calculations discussed here we assume that the hadron attenuation effects are already corrected for (or are negligible). As can be seen in Fig. 4, the ratio of the difference of charge states as well as the double-ratio of π^+/π^- for each target show significant sensitivity to the flavor dependence of the EMC effect. The ratio of the difference of yields for π^+ and π^- production shows a slightly larger effect, however as noted earlier, this approach requires

an explicit correction for hadron attenuation effects. The ratio of charged pion yields also shows slightly smaller sensitivity, but still a potentially significant effect, and is easier to measure precisely experimentally. In addition, this latter approach merely requires the same or similar hadron attenuation effects for π^+ and π^- production.

C. Medium Modifications of the Fragmentation Functions

In analogy with the parton distribution functions, the fragmentation functions depend on a scaling variable, and in this case it is z instead of x . In the quark parton model, the fragmentation functions are approximately equivalent to hadron multiplicities. The hadrons multiplicity for hadron species h is defined as,

$$M_h(z) = \frac{1}{\sigma_e} \frac{d\sigma_h}{dzd\nu} = \frac{\sum_f e_f^2 q_f(x) D_f^h(z)}{\sum_f e_f^2 q_f(x)}, \quad (12)$$

where σ_e is the inclusive electron scattering cross section. In QCD the relationship between the fragmentation functions and the multiplicities is more complicated, however, the HERMES experiment has shown [19] that by integrating over a broad range of x the hadron multiplicities in semi-inclusive DIS are in good agreement with the QCD evolution of the fragmentation functions determined from e^+e^- measurements at CERN ([15] and references therein).

Similar to the EMC effect, where the parton distributions functions are modified in the nuclear medium, the fragmentation function can/are also modified in the nuclear medium. One can study the medium modification of the fragmentation function by using semi-inclusive DIS measurements on nuclei. The nucleus acts as an ensemble of targets which reduce the multiplicity of fast hadrons due to hadronic interactions. This is called hadron attenuation. Hadron attenuation effects have been studied at EMC [20], HERMES [21], and more recently at JLab [22]. In these experiments, the nuclear dependence of semi-inclusively produced hadrons is used to study hadron production and formation times. The hadron attenuation ratio for a hadron species h is defined as,

$$R_h(z, \nu) = \frac{\left(\frac{1}{\sigma} \frac{d\sigma}{dzd\nu}\right)_A}{\left(\frac{1}{\sigma} \frac{d\sigma}{dzd\nu}\right)_D} = \frac{\left(\frac{1}{N_e} \frac{dN_h}{dzd\nu}\right)_A}{\left(\frac{1}{N_e} \frac{dN_h}{dzd\nu}\right)_D}. \quad (13)$$

Here, the inclusive cross section has been explicitly removed such that one is only probing modifications to the formation of hadrons in the nucleus and not differences in the “initial state” quark distributions. It is clear that hadron attenuation will play an important role in any experiment using the nuclear dependence of semi-inclusive pion production to probe the EMC Effect. As can be seen in Fig. 5, the nuclear environment can have significant effects

the formation of hadrons. At very large ν , such effects are seen to be small, but the required ν values ($\approx 10 - 20$ GeV) are not accessible at JLab.

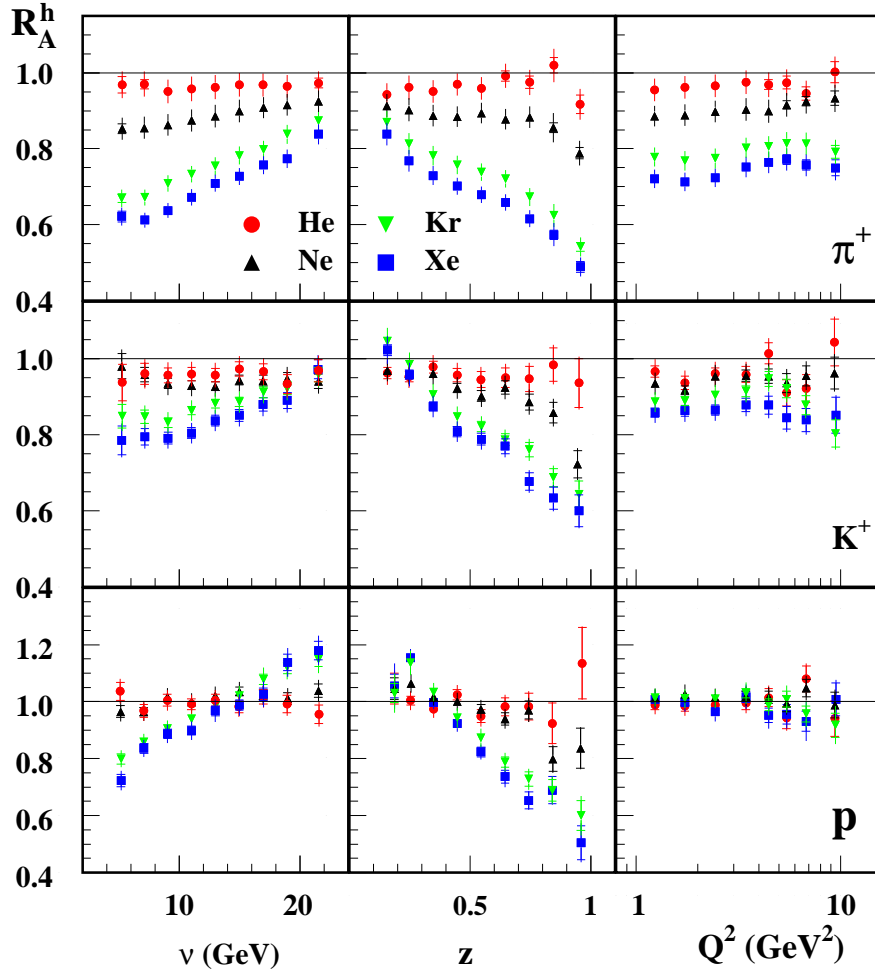


FIG. 5: Hadron attenuation ratios as measured at HERMES [21]. Here we show one sample plot for positively charged hadrons - similar results for negatively charged hadrons also can be found in Ref. [21].

Our strategy to alleviate (or at least minimize) effects from hadron attenuation in nuclei compared to deuterium is as follows.

1. When measuring the charged pion yield super-ratio, $[Y_A(\pi^-)/Y_A(\pi^+)]/[Y_D(\pi^-)/Y_D(\pi^+)]$, effects from hadron attenuation should mostly cancel to the extent that such attenuation effects are the same for both π^+ and π^- (this has been observed at the few percent level at HERMES).
2. We also plan to precisely map out hadron attenuation effects as a function of both z and ν for both charge states at $x = 0.3$, where there is no EMC Effect and we are sure

that any differences between the two charge states does not come from a difference in the nuclear quark distributions. To the extent that the two charge states yield different attenuation effects at $x = 0.3$, we can apply the measured difference as a correction to our measurements at larger x .

Finally, it is worth noting that to the extent that we can measure the absolute value of the hadron attenuation ratio, we can apply this as an explicit (large) correction to the ratio of charge differences, $[Y(\pi^+ - \pi^-)_A]/[Y(\pi^+ - \pi^-)_D]$. Additionally, the gold to deuterium ratio of the charged pion yield sum $(\pi^+ + \pi^-)$ will provide a useful check that these effects are under control since this ratio should simply reproduce the ratio of inclusive structure functions. However, there will certainly be a slightly larger uncertainty in the final result in the ratio of the difference of charge states due to hadron attenuation effects.

VI. FACTORIZATION AT A 12 GEV JLAB

One assumption implicit in the formalism of the previous sections is that of independent fragmentation, i.e., that semi-inclusive pion production can be described by two independent processes. First, the virtual photon interacts with a quark in the hadronic system - then that quark subsequently hadronizes forming a pion or other particle. Only when this picture is valid can we be confident that we are really probing the quark flavor dependence of the EMC effect.

It is not a foregone conclusion that semi-inclusive processes at a 12 GeV JLab will satisfy the factorization criteria described above, however there is good reason to believe that it may. Already at 6 GeV, we have seen signs that factorization may be satisfied. Figs. 6 and 7 show results from Hall C experiment 00-108 [23] in which semi-inclusive charged pion production from hydrogen and deuterium targets was measured. In this experiment, the absolute cross sections were found to be consistent with cross section calculations performed in a leading order framework using Cteq5 [24] parton distribution functions and a high energy parameterization of the fragmentation functions[15] (see Fig. 6). In addition, the z dependence of combinations of the two charge states and targets was also examined. If independent fragmentation holds, then the following relations should hold true, independent of z :

$$\frac{\sigma_p(\pi^+) + \sigma_p(\pi^-)}{\sigma_d(\pi^+) + \sigma_d(\pi^-)} = \frac{4u(x) + 4\bar{u}(x) + d(x) + \bar{d}(x)}{5[u(x) + d(x) + \bar{u}(x) + \bar{d}(x)]} \quad (14)$$

and

$$\frac{\sigma_p(\pi^+) - \sigma_p(\pi^-)}{\sigma_d(\pi^+) - \sigma_d(\pi^-)} = \frac{4u_v(x) - d_v(x)}{3[u_v(x) + d_v(x)]}. \quad (15)$$

These ratios are plotted in Fig. 7 and are found to be consistent with the simple factorization assumption up to $z \approx 0.7$.

While the Hall C 6 GeV results are promising, it is important to test for factorization over a wider kinematic range, and especially at the kinematics relevant to this experiment. We plan to perform tests similar to those performed in E00–108 to verify that factorization is satisfied.

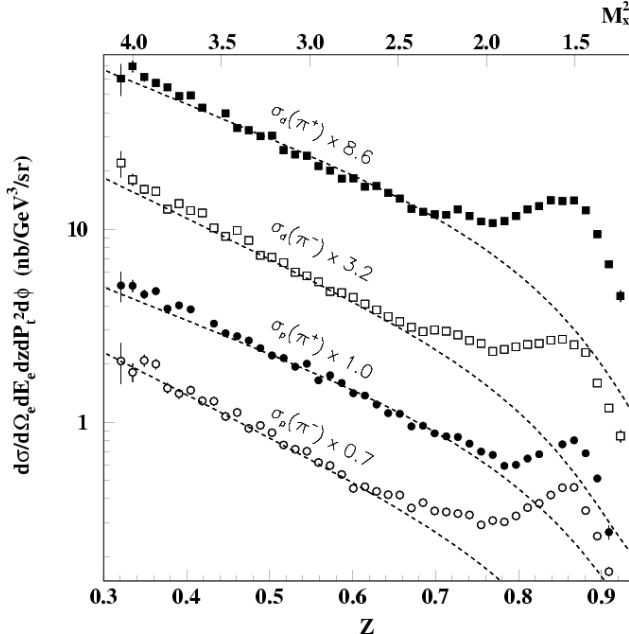


FIG. 6: Cross sections for $H, D(e, e'\pi^\pm)$ from Hall C experiment 00–108. Curves denote calculations using a simple factorization picture as described in the text. Closed symbols have been corrected for backgrounds from exclusive ρ production.

VII. EXPERIMENTAL OVERVIEW

Since the effect we are attempting to measure is potentially small, it is important that systematic errors are well controlled. In particular, since we will be comparing yields of negatively and positively charged pions, it is crucial that the acceptance for detection of the charged pion is independent of pion charge. For this reason, magnetic, focusing spectrometers hold a clear advantage over large acceptance devices that may have non-charge symmetric acceptance effects. In addition, small angles and large momenta are required, hence Hall C with the HMS and new SHMS are well suited to this experiment.

A. Kinematics

This experiment will measure semi-inclusive pion electroproduction from gold and deuterium at large x to map out potential flavor differences in the EMC Effect. The kinematics

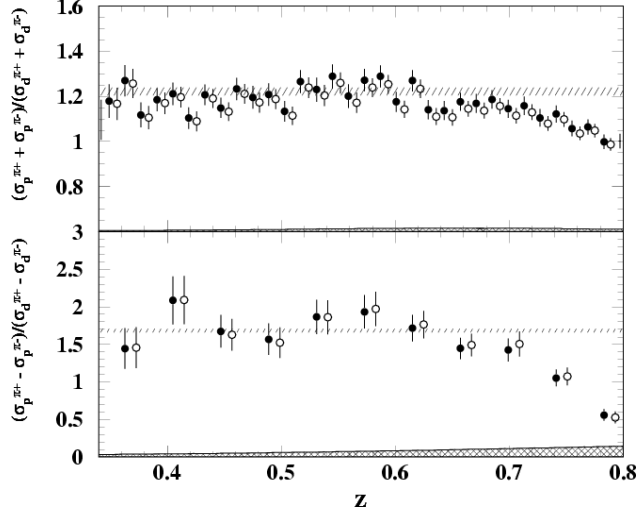


FIG. 7: Ratio of proton to deuteron results for the sum (top) and difference (bottom) of the π^+ and π^- cross sections. The ratios are independent of z up to $z \approx 0.7$.

were chosen with the following goals:

- Measure semi-inclusive charged pion electroproduction from $x = 0.2$ to $x = 0.6$ at a fixed $z = 0.5$. This will allow us to fully map the x dependence of flavor-dependent effects over the “EMC Effect” region.
- At $x = 0.3$, semi-inclusive yields will be measured for a variety of z and ν to map out hadron attenuation effects where the EMC Effect is small. Here, we will test precisely whether hadron attenuation effects for π^+ and π^- production are identical, and to the extent that they are not, measure the difference in order to correct our results at larger x .
- At $x = 0.5$, map out the z dependence of the semi-inclusive pion yields. This will allow us to test our sensitivity to particular models of fragmentation functions.
- Measurements at $x = 0.5$ and $x = 0.6$ will be made at approximately the same Q^2 to minimize systematic errors in the extraction of the charge symmetry violating quark distributions discussed in our companion experiment [26].

In addition, to the above criteria, we require the usual “DIS” kinematics such that $Q^2 > 1 \text{ GeV}^2$ and $W^2 > 4 \text{ GeV}^2$. Also, we will require $W'^2 = (m_p + \nu - E_\pi)^2 - |\vec{q} - \vec{p}_\pi|^2$, the mass of the unobserved final state, be larger than 2.5 GeV^2 . This last constraint is driven by the observation from E00-108 that factorization seems to hold up to $z = 0.7$, or for their kinematics, $W'^2 > 2.5 \text{ GeV}^2$.

This experiment will measure $D(e, e'\pi^+)X$, $D(e, e'\pi^-)X$, $Au(e, e'\pi^+)X$, and $Au(e, e'\pi^-)X$ using the HMS and SHMS spectrometers in Hall C. Electrons will be detected in the SHMS and the charged pions in the HMS. The proposed kinematics for this experiment are shown in Table I. Electron momenta and angles range from 4.5 to 6.5 GeV and 10.22° to 20.21° respectively while pion kinematics require momenta from 1.88 to 4.55 GeV and angles of 10.51° to 17.02° . These requirements are well within the capabilities of the SHMS and HMS. Note that the minimum separation of 17.5° between both spectrometers is always satisfied.

Q^2 (GeV ²)	ν (GeV)	W (GeV)	θ_e (deg)	E_e (GeV)	θ_q (deg)	z	W'^2 (GeV ²)	P_π (GeV)
$x = 0.2$								
1.99	5.3	2.97	10.22	5.7	10.62	0.5	4.82	2.12
$x = 0.3$								
3.55	6.3	3.02	15.05	4.7	10.70	0.4	5.79	2.52
						0.5	4.96	3.15
						0.6	4.13	3.78
						0.7	3.30	4.41
2.53	4.5	2.61	10.80	6.5	14.78	0.5	3.77	2.25
2.81	5.0	2.73	11.85	6.0	13.51	0.5	4.10	2.50
3.10	5.5	2.85	12.99	5.5	12.36	0.5	4.44	2.75
3.38	6.0	2.96	14.23	5.0	11.30	0.5	4.77	3.00
3.38	6.4	3.05	15.32	4.6	10.51	0.5	5.02	3.20
$x = 0.4$								
3.53	4.7	2.48	12.95	6.3	16.20	0.5	3.44	1.88
$x = 0.5$								
6.10	6.5	2.64	20.21	4.5	12.92	0.4	4.25	2.60
						0.5	3.81	3.25
						0.6	3.18	3.90
						0.7	2.56	4.55
$x = 0.6$								
6.08	5.4	2.22	18.07	5.6	17.02	0.5	2.73	2.16

TABLE I: Kinematics proposed for this measurement.

B. Coincidence and Singles Rate Estimates

Rates for the $D(e, e'\pi^+)X$, $D(e, e'\pi^-)X$, $Au(e, e'\pi^+)X$, and $Au(e, e'\pi^-)X$ reactions have been estimated using SIMC, the standard Hall C Monte Carlo package. This simulation includes effects from radiative processes, pion decay, multiple scattering, as well as detailed models of the SHMS and HMS acceptances. It should be noted that the SHMS component of SIMC has not yet been updated to reflect the most recent revisions to the SHMS design. In the Monte Carlo, the SHMS has an approximate solid angle of 3.5 msr and momentum bite of 35%, however, the updated design yields a larger solid angle of 5.0 msr with a slightly smaller momentum bite of 32%. For our rate estimates, we take the nominal SIMC yield and scale by $5/3.5 \times 32/35 = 1.3$ to account for the new SHMS design.

The model used for the semi-inclusive process is the same as described in Fig. 4, i.e., MRST01-LO parton distributions and Nuclear PDFs of Ref. [14], combined with fragmentation function information from Refs. [15] and [16]. In addition, hadron attenuation effects in gold have been taken into account using results from HERMES as a guide.

Coincidence yields are for a 10 cm long liquid deuterium target and 6% radiation length (0.3876 g/cm^2) gold target. Additional data for factorization tests will be taken at $x = 0.3$ and $x = 0.5$ using a 10 cm hydrogen target.

At each setting, care has been taken to keep the total particle yield (including singles rates) in the hadron arm the same for both π^+ and π^- running. This helps reduce the systematic error associated with rate dependent effects in the particle tracking efficiency, as well as potential rate dependent effects in other detectors.

Singles rates for hadrons (π^\pm, K^\pm , and protons) produced from the liquid deuterium target have been estimated using the parameterization from Wiser [29]. Electron rates have been calculated using a fit to SLAC proton and deuterium data, taking into account the EMC effect where appropriate. In general, the singles rates in the hadron arm (the HMS) are rather high, and in particular, are about a factor of two larger for positive polarity as compared to negative polarity. In order to minimize the difference between rate dependent inefficiencies (the primary one being the tracking efficiency), we assume that the positive polarity running will be at half the current as the negative polarity running.

Since the Wiser fit applies only to proton and deuterium targets, we were not able to use it to estimate the singles rates for the 6% gold target. However, it was observed during Hall C experiment E01-107 (a measurement of pion transparency in nuclei) that singles rates in the hadron arm from a 6% gold target were approximately the same as those from a 4 cm cryotarget. Therefore, we expect the singles rates from gold for this experiment to be about 2.5 times smaller than those from the 10 cm liquid deuterium target, assuming the same beam current.

In general we assume $50 \mu A$ beam current at negative polarity, so the positive polarity running will be at $25 \mu A$. At the kinematic settings where the singles rates exceed 1 MHz for

these nominal currents, the beam current is further reduced to $30 \mu A$ and $15 \mu A$ for negative and positive polarity respectively (accounted for in the beam-time table IX). Singles rates in the HMS are shown in Table II and in the SHMS are shown in Table III and the coincidence rates are shown in Table IV.

			Positive polarity				Negative Polarity			
x	z	ν	π^+	K^+	p	Total +	e^-	π^-	K^-	Total -
(GeV)			(MHz)	(MHz)	(MHz)	(MHz)	(MHz)	(MHz)	(MHz)	(MHz)
0.2	0.5	5.3	0.87	0.15	0.25	1.27	0.06	1.13	0.07	1.28
0.3	0.4	6.3	0.97	0.16	0.28	1.40	0.06	1.25	0.08	1.40
0.3	0.5	6.3	0.49	0.10	0.16	0.75	0.07	0.66	0.05	0.79
0.3	0.6	6.3	0.24	0.06	0.08	0.38	0.08	0.32	0.03	0.43
0.3	0.7	6.3	0.11	0.03	0.04	0.18	0.09	0.15	0.01	0.25
0.3	0.5	4.5	0.43	0.08	0.20	0.71	0.02	0.57	0.04	0.63
0.3	0.5	5.0	0.44	0.08	0.18	0.70	0.02	0.58	0.04	0.65
0.3	0.5	5.5	0.45	0.09	0.17	0.71	0.04	0.60	0.04	0.69
0.3	0.5	6.0	0.47	0.10	0.16	0.73	0.05	0.64	0.05	0.74
0.3	0.5	6.4	0.50	0.11	0.15	0.76	0.07	0.67	0.05	0.80
0.4	0.5	4.7	0.25	0.05	0.14	0.43	0.01	0.33	0.02	0.37
0.5	0.4	6.5	0.46	0.09	0.18	0.73	0.03	0.61	0.04	0.69
0.5	0.5	6.5	0.19	0.05	0.08	0.32	0.03	0.26	0.02	0.32
0.5	0.6	6.5	0.07	0.02	0.03	0.13	0.04	0.10	0.01	0.15
0.5	0.7	6.5	0.03	0.01	0.01	0.05	0.04	0.04	0.04	0.11
0.6	0.5	5.4	0.10	0.02	0.07	0.19	0.01	0.14	0.01	0.17

TABLE II: Singles rates in the HMS (hadron arm) at positive and negative polarity from deuterium. Rates are calculated assuming a 10 cm liquid deuterium target and a beam current of 25 (50) μA at positive (negative polarity). Different beam currents are used for the positive and negative polarity to keep the total event rate in the HMS roughly constant between the two polarities. Singles rates for the 6% gold target are expected to be about 2.5 times smaller based on previous experience in Hall C.

C. Particle Identification

This experiment has relatively modest particle identification requirements which should be easily achievable using the standard detectors in the HMS and SHMS spectrometers.

We will be detecting electrons with momenta ranging from 4.5 to 6.5 GeV in the SHMS. The SHMS has available a lead–glass calorimeter, a heavy-gas Čerenkov detector (intended

			10 cm LD2				6% Gold			
x	z	ν	π^-	K^-	e	Total	π^-	K^-	e	Total
			(kHz)	(kHz)	(kHz)	(kHz)	(kHz)	(kHz)	(kHz)	(kHz)
0.2	0.5	5.3	33.5	3.2	143.6	180.3	13.4	1.3	32.8	47.5
0.3	0.4-0.7	6.3	7.9	0.8	19.8	28.5	3.2	0.3	4.4	7.9
0.3	0.5	4.5	6.1	0.5	120.7	127.3	2.4	0.2	26.9	29.5
0.3	0.5	5.0	6.3	0.6	71.9	78.8	2.5	0.2	16.0	18.8
0.3	0.5	5.5	6.7	0.7	43.4	50.8	2.7	0.2	9.7	12.7
0.3	0.5	6.0	7.4	0.7	26.6	34.7	3.0	0.3	5.9	9.1
0.3	0.5	6.4	8.2	0.8	18.0	27.0	3.3	0.3	4.0	7.6
0.4	0.5	4.7	1.4	0.1	40.9	42.4	0.6	0.0	8.8	9.4
0.5	0.4-0.7	6.5	0.5	0.0	2.8	3.33	0.2	0.0	0.6	0.8
0.6	0.5	5.4	0.1	0.0	3.6	3.69	0.0	0.0	0.7	0.8

TABLE III: Singles rates in the SHMS (electron arm) from a 10 cm deuterium target and 6% gold target. π^- and K^- rates for gold are estimated by scaling the deuterium rates by a factor of 1/2.5. The assumed beam current is 50 μA , although the π^+ running will be at only 25 μA . Note that the total rate in the SHMS is low enough (always less than 200 kHz) that uncertainties due to rate dependent efficiency differences should be minimal.

primarily for pion detection, however it can be configured for modest pion rejection at these momenta), and an atmospheric Čerenkov detector (see Fig. 8). We estimate that the π^- rates will be relatively modest (10's of kHz), so pion rejection will not be too difficult. The planned lead-glass calorimeter for the SHMS, which will have > 99% electron detection efficiency with $\approx 200:1$ pion rejection [25], is almost sufficient for our purposes on its own. However, we will also make use of the heavy gas Čerenkov operated at < 1atm to further reduce the pion background.

The electroproduced pions will be detected in the HMS with momenta ranging from 1.9 to 4.6 GeV. This momentum range is similar to that for Hall C Experiment 01-107 [27, 28]. In that case, pions were identified using a combination of gas Čerenkov and aerogel detectors. The HMS gas Čerenkov contained C_4F_{10} at a pressure of 0.96 atm. This yields a pion threshold of 2.65 GeV (kaon threshold of 9.4 GeV) so can reliably be used to separate positively charge pions from kaons and protons. At lower momenta, an aerogel with index of refraction $n = 1.015$ was used (pion threshold = 0.8 GeV). Kaon threshold for this detector is 2.85 GeV, hence pions can be cleanly identified over the full range of momenta accessed in this experiment.

Schematically, our pion identification strategy can be summarized:

x	z	ν	π^+ (Hz)	π^- (Hz)	π^+ (Hz)	π^- (Hz)
		(GeV)	deuterium		gold	
0.20	0.50	5.3	95.23	123.86	9.27	12.36
0.30	0.40	6.3	14.26	19.10	1.36	1.89
0.30	0.50	6.3	15.84	19.84	1.49	1.94
0.30	0.60	6.3	15.43	18.13	1.42	1.76
0.30	0.70	6.3	12.47	13.84	1.16	1.36
0.30	0.50	4.5	61.97	78.45	5.78	7.60
0.30	0.50	5.0	47.49	59.69	4.49	5.87
0.30	0.50	5.5	35.96	45.08	3.43	4.48
0.30	0.50	6.0	26.51	33.18	2.52	3.30
0.30	0.50	6.4	19.50	24.41	1.85	2.42
0.40	0.50	4.7	14.87	18.46	1.28	1.68
0.50	0.40	6.5	1.57	2.07	0.13	0.18
0.50	0.50	6.5	1.74	2.14	0.14	0.18
0.50	0.60	6.5	1.65	1.88	0.13	0.16
0.50	0.70	6.5	1.35	1.45	0.10	0.12
0.60	0.50	5.4	1.23	1.52	0.09	0.12

TABLE IV: Coincidence rates from a 10 cm deuterium target and 6% gold target. π^- rates are for 50 μA and π^+ are at 25 μA .

1. $P_{HMS} = 1.9 - 2.62$ GeV: Pions will fire the $n = 1.015$ aerogel. At $P_{HMS} = 2.62$ GeV, the momentum bite of the HMS will accept particles up ≈ 2.83 GeV, still below kaon threshold (2.85 GeV) for this detector.
2. $P_{HMS} = 2.86 - 4.55$ GeV: Pions will fire the C_4F_{10} gas Čerenkov at 0.96 atm (threshold=2.65 GeV) while kaons will not. Kaons will, however, begin to fire the aerogel detector.
3. Electrons in the HMS at negative polarity will be rejected by the lead-glass calorimeter, aided by the C_4F_{10} gas Čerenkov below central momenta of 2.62 GeV.

Note that one setting at $P_{HMS} = 2.75$ GeV falls in the gap where the HMS Čerenkov will begin to fire for pions in part of the acceptance ($\delta > -3.5\%$) while the aerogel will begin to fire for kaons in part of the acceptance ($\delta > 3.6\%$). In this case, if the kaon backgrounds are found to be too large, we can limit the HMS momentum acceptance (on either the high or low end) to ensure clean pion identification.³

³ Alternatively, one can operate the HMS Čerenkov at a pressure larger than 1 atm. to lower the pion

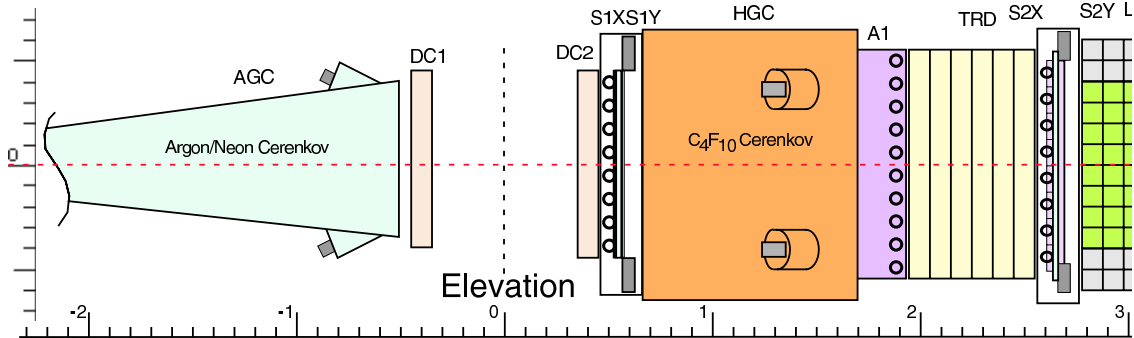


FIG. 8: Schematic of the planned detector stack in the SHMS. An optional Argon–Neon Čerenkov placed before the drift chambers will not be used for this experiment since the lead–glass calorimeter and heavy gas Čerenkov will be sufficient to reject the relatively modest rate of charged pions in the SHMS.

When detecting negatively charged pions in the HMS, we must also reject electrons. The HMS calorimeter electron rejection can be as large as 100:1 at 1 GeV and 1000:1 at 2 GeV with a pion detection efficiency larger than 99.5%. This is more than adequate for the maximum 90 kHz electron rates we expect in the HMS.

VIII. ρ AND $N(e, e'\pi^\pm)N'$ RADIATIVE BACKGROUNDS

In addition to semi-inclusive production of charged pions, pions from the decay of diffractively produced ρ particles and pions produced exclusively at $z = 1$ that “radiate in” to the spectrometer acceptance will also contribute to the measured yield. Our estimate of the contribution of these processes to our measured signal is summarized in Table V and Figures 9 and 10.

The contribution from diffractive ρ production was estimated using the ρ cross section from PYTHIA [30] modified to agree with HERMES data [31] with additional modifications to agree with recent CLAS data [32] at lower energies. In general, we find that the contribution from diffractive ρ production is not large ($< 10\%$) at the kinematics of the $z \approx 0.5$ x -scan. At the largest z values ($z = 0.7$), however, this fraction can grow to 20%. To estimate the uncertainty on our extracted signal, the super-ratio of charged pion yields for each target, we assume the parameterization of the ρ cross section used in the simulation is accurate to about 20%. The uncertainty on the contribution to the yield of π^+ events from

threshold slightly. While the Čerenkov detector has been designed with this capability in mind, there is a certain degree of inconvenience in that the entrance and exit windows of the detector must be removed and flipped.

deuterium, for example, is then 1.34% (at $x = 0.2$) to 0.68% (at $x = 0.6$) for the $z = 0.5$ data. However, contribution to this uncertainty to the π^+/π^- ratio is reduced due to the fact that the yield for π^- events from diffractive ρ production should be identical to that from π^+ events. Hence, in the charge ratio for a single target, the uncertainty is reduced to 0.55% (at $x = 0.2$) to 0.40% (at $x = 0.6$). To be conservative, we assume this uncertainty for a single target is uncorrelated to the uncertainty in the other target and hence the total contribution to the uncertainty on the super-ratio is amplified by $\sqrt{2}$ yielding 0.78% to 0.57%.

It is worth noting that when calculation the ratio of the difference of yields ($\pi^+ - \pi^-$) this background ρ production subtracts away and contributes minimally to the uncertainty in that quantity.

			$Y(\rho \rightarrow \pi^+\pi^-)/Y(e'\pi X)$		$Y(e'\pi N\gamma)/Y(e'\pi X)$	
x	z	ν (GeV)	π^+	π^-	π^+	π^-
0.2	0.5	5.3	0.067	0.10	0.026	0.026
0.3	0.4	6.3	0.027	0.039	0.010	0.005
0.3	0.5	6.3	0.042	0.066	0.034	0.022
0.3	0.6	6.3	0.060	0.101	0.027	0.016
0.3	0.7	6.3	0.098	0.176	0.056	0.039
0.3	0.5	4.5	0.074	0.112	0.043	0.028
0.3	0.5	5.0	0.067	0.103	0.040	0.026
0.3	0.5	5.5	0.060	0.091	0.038	0.025
0.3	0.5	6.0	0.055	0.084	0.035	0.023
0.3	0.5	6.4	0.050	0.079	0.034	0.022
0.4	0.5	4.7	0.049	0.079	0.035	0.021
0.5	0.4	6.5	0.021	0.031	0.007	0.003
0.5	0.5	6.5	0.031	0.050	0.043	0.019
0.5	0.6	6.5	0.047	0.082	0.027	0.012
0.5	0.7	6.5	0.074	0.139	0.063	0.030
0.6	0.5	5.4	0.034	0.056	0.040	0.016

TABLE V: Fractional contribution to the yield of semi-inclusive pions produced from deuterium from pions resulting from the decay of diffractively produced rho, and the radiative tail from exclusive pion production.

The yield of events from the radiative tail from exclusive pion production (i.e. $e + p(n) \rightarrow e' + \pi^\pm n(p) + \gamma$) was estimated using radiative effects implemented in the energy peaking approximation in SIMC combined with a fit to exclusive pion electroproduction for W above the resonance region [33, 34] modified to reproduce the general features of the

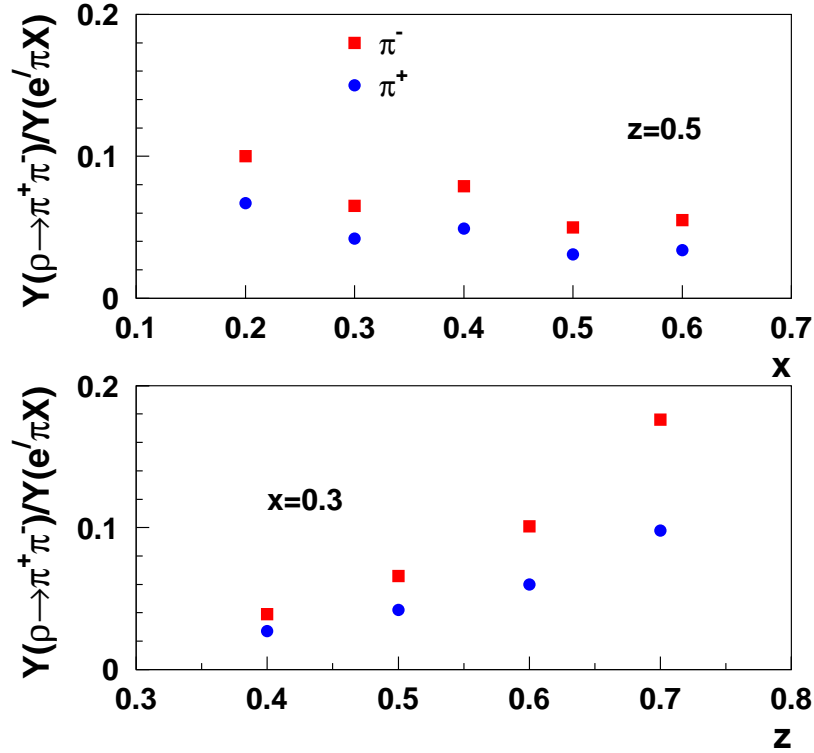


FIG. 9: Contribution of pions coming from the decay of diffractively produced ρ particles to the semi-inclusive yield of π^+ from deuterium. The top panel shows the fraction for the “ x -scan” kinematics at fixed z (see Table I, while the bottom panel shows the fraction as a function of z at fixed $x = 0.3$.

MAID model [35] at lower W . In general, contributions from these events are quite small, never more than 5% for the x -scan data at fixed z , while growing to $\approx 7\%$ at the largest z sampled in this experiment.

Although the total contribution to the yield is smaller when compared to that from diffractive ρ production, the net contribution to the uncertainty in the super-ratio is comparable. If we again assume that the cross section model used to generate the radiated events is good to 20%, then the uncertainty on the contribution to the yield is $\approx 0.7\%$ for π^+ and 0.4% for π^- (assuming 3.5% and 2% as representative, “typical” fractions for the x -scan data). However, these uncertainties are largely uncorrelated between charge states, resulting in an uncertainty of 0.8% for the charge ratio for a given target. When determining the super-ratio, the result will not be amplified since the same difference in exclusive π^+ and π^- cross sections applies to both targets. To be conservative however, we estimate the total

contribution to the uncertainty in the super-ratio to be about 1%.

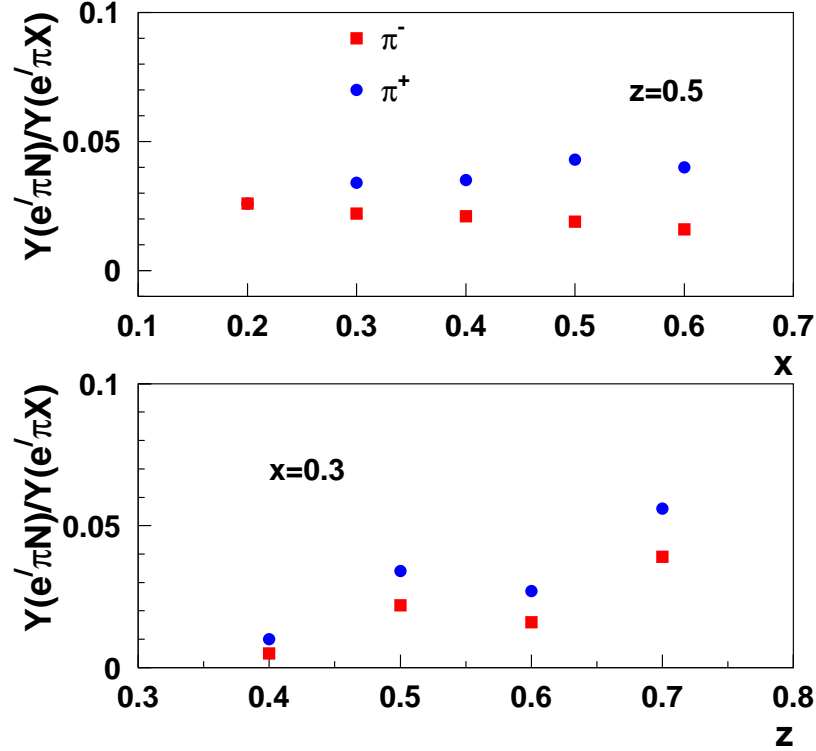


FIG. 10: Contribution from the radiative tail of exclusive pion production to semi-inclusive π^+ production from deuterium. Top and bottom panels are as described in Figure 9.

IX. UNCERTAINTIES AND PROJECTED RESULTS

At each setting, we will take enough statistics to achieve $\approx 1.5\%$ uncertainties in the charged pion super-ratio, $R_{Au/D}^{\pi^+/\pi^-} = [Y_{Au}(\pi^+)/Y_{Au}(\pi^-)]/[Y_D(\pi^+)/Y_D(\pi^-)]$. Given the significant backgrounds from random coincidences (the ratio of real to random coincidences will be on the order of 1.0 for the x -scan data at $z = 0.5$, see Table VI), we in general need to take 40,000 events at each setting for each target and polarity. For the gold data at larger x , we are able to take fewer events due to relatively favorable signal to noise without undue effect on the overall uncertainty. In addition, we take fewer events on both gold and deuterium targets at $x = 0.5$, for $z = 0.4, 0.6,$ and 0.7 . The statistics goals at each setting are summarized in Table VII.

x	z	ν (GeV)	I_e (μA)	π (kHz)	e^- (kHz)	Random (Hz)	Real (Hz)	$\frac{\text{Real}}{\text{Random}}$	I_e (μA)	π (kHz)	e^- (kHz)	Random (Hz)	Real (Hz)	$\frac{\text{Real}}{\text{Random}}$
			π^+						π^-					
0.20	0.50	5.3	15	520	43.1	44.8	57.1	1.3	30	680	86.2	117.3	74.3	0.6
0.30	0.40	6.3	15	579	5.9	6.9	8.6	1.2	30	752	11.9	17.9	11.6	0.7
0.30	0.50	6.3	25	493	9.9	9.8	15.8	1.6	50	664	19.8	26.3	19.8	0.8
0.30	0.60	6.3	25	235	9.9	4.6	15.4	3.3	50	324	19.8	12.8	18.1	1.4
0.30	0.70	6.3	25	105	9.9	2.1	12.5	6.0	50	148	19.8	5.9	13.8	2.4
0.30	0.50	4.5	25	433	60.4	52.3	62.0	1.2	50	568	120.7	137.1	78.5	0.6
0.30	0.50	5.0	25	438	36.0	31.5	47.5	1.5	50	580	71.9	83.4	59.7	0.7
0.30	0.50	5.5	25	451	21.7	19.6	36.0	1.8	50	602	43.4	52.3	45.1	0.9
0.30	0.50	6.0	25	474	13.3	12.6	26.5	2.1	50	637	26.6	33.9	33.2	1.0
0.30	0.50	6.4	25	500	9.0	9.0	19.5	2.2	50	673	18.0	24.2	24.1	1.0
0.40	0.50	4.7	25	249	40.9	10.2	14.9	1.5	50	332	40.9	27.2	18.5	0.7
0.50	0.40	6.5	25	458	1.4	1.3	1.6	1.2	50	609	2.8	3.4	2.1	0.6
0.50	0.50	6.5	25	189	1.4	0.5	1.7	3.3	50	260	2.8	1.5	2.1	1.5
0.50	0.60	6.5	25	72	1.4	0.2	1.7	8.2	50	102	2.8	0.6	1.9	3.3
0.50	0.70	6.5	25	25	1.4	0.1	1.4	19.3	50	36	2.8	0.2	1.5	7.2
0.60	0.50	5.4	25	104	1.8	0.4	1.2	3.3	50	143	3.6	1.0	1.5	1.5

TABLE VI: Estimate of ratio of real to random coincidences for a 10 cm deuterium target. Rates are shown for actual currents to be used in data-taking. It is assumed that the singles rates contributing to the random coincidences come from the particle species of interest, i.e. pions in the HMS and electrons in the SHMS. Random coincidence rates are estimated assuming a 2 ns coincidence window. The amplification of the statistical error will be non-trivial due to the significant random backgrounds; for the x -scan data at fixed, the ratio of real to random coincidences is on the order of 1. The real to random ratio for the gold running is not shown, but is similar at each setting.

Uncertainties due to backgrounds from diffractive ρ production and the radiative tail of exclusive pion production have already been discussed above and are the largest systematic uncertainties in this experiment. Many experimental systematic uncertainties, such as absolute target thickness, pion re-scattering and absorption in the spectrometer, while potentially different for each charge state will also cancel in the double ratio.

Other notable sources of uncertainty come from the measurement of beam current and boiling effects in the liquid deuterium target. The dominant contribution to the uncertainty in the measurement of the beam current comes from the ≈ 200 nA noise in the Unser monitor used to calibrate the hall resonating cavity monitors. This leads to a 0.8% (0.4%) uncertainty at the 25 μA (50 μA) used for the π^+ (π^-) running. However, this 200 nA is common to

			Deuterium		Gold	
x	z	ν (GeV)	N_{π^+}	N_{π^-}	N_{π^+}	N_{π^-}
0.2	0.5	5.3	40k	40k	40k	40k
0.3	0.4-0.7	6.3	40k	40k	40k	40k
0.3	0.5	4.5-6.4	40k	40k	40k	40k
0.4	0.5	4.7	40k	40k	40k	40k
0.5	0.4	6.5	20k	20k	10k	10k
0.5	0.5	6.5	40k	40k	20k	20k
0.5	0.6	6.5	20k	20k	10k	10k
0.5	0.7	6.5	20k	20k	10k	10k
0.6	0.5	5.4	40k	40k	20k	20k

TABLE VII: Statistics goals for each setting. We expect $\approx 1.5\%$ statistical precision for each x setting of the $z = 0.5$ scan. Larger numbers of events are required due to the $\approx 1 : 1$ real to random coincidence ratio. We take fewer events for the extra z setting at $x = 0.5$ since these data are primarily for systematic checks.

both measurements and so only contributes in as much as the current between each charge state is different. Hence the uncertainty on the current measurement in the single target charge ratio is 0.4%. Once the double-ratio is formed, this contribution completely drops out. The only remaining uncertainty is then due to the ability to monitor the relative gains of the BCM, which is usually good to 0.1%. Target boiling effects in long cryogenic targets have been observed several times in Hall C. The reduction of luminosity due to these effects varies linearly with beam current. We expect that we will be able to measure this reduction using high-rate inclusive processes to at least 1%. Since the beam currents between pion charge states changes by only a factor of two, this contributes 0.5% to the charge ratio.

As discussed earlier, uncertainties due to differences in tracking efficiencies, a potentially large correction at the high single-arm rates of this experiment, will be mitigated by keeping the singles rates in the hadron arm close to identical. The rates in the electron arm will necessarily be different, but since the global rates are much lower (at most 130 kHz) uncertainties associated with tracking are much smaller.

Other uncertainties due to particle ID efficiency and acceptance should almost completely cancel in the super-ratio, but we include allowance for some small difference, perhaps due to slightly different event distributions across the spectrometer acceptance.

We estimate the total systematic uncertainty in the super-ratio to be $\frac{dR}{R} = 1.3 - 1.4\%$.

The projected results for the π^+/π^- super-ratio and the difference ratio are shown in Fig. 11 for the x scan at $z = 0.5$ setting. We also show the projected results for the z scan at $x = 0.5$ in Fig. 12. The projections for the z scan at $x = 0.3$ and the ν scan at

Source	Uncertainty	Uncertainty in $R_{Au/D}^{\pi^+/\pi^-}$
Statistics	0.7%	1.5%
Beam current	0.4 -0.8%	0.1%
Target boiling (D2)	<1%	0.5%
Tracking efficiency	0.1-1%	0.2%
Dead time	<0.1%	<0.1%
Acceptance	1-2%	0.1%
PID efficiency	<0.5%	0.2%
ρ backgrounds	0.5-1.3%	0.57-0.78%
Exclusive rad. tail	0.4-0.7%	1.0%
Total systematic		1.3-1.4%
Total uncertainty	–	2.0-2.1%

TABLE VIII: Dominant systematic uncertainties on the super-ratio of π^+/π^- yields between gold and deuterium.

$x = 0.3$ and $z = 0.5$ are shown in Fig. 13. At $x = 0.3$ since there is no EMC effect, there is no flavor dependence either. Both the z scan and the ν scan at $x = 0.3$ will be used to help quantify hadron attenuation and used to correct (if required) the difference and super-ratio at higher x . These projected results demonstrate the great promise held by the new observables introduced in this proposal to unraveling any flavor dependence of the EMC effect and also demonstrate the precision of the semi-inclusive DIS measurements that will be accessible at the upgraded Hall-C.

X. RELATION TO OTHER EXPERIMENTS

The primary observable in this experiment, the charged-pion super-ratio, $R_{Au/D}^{\pi^+/\pi^-} = (Y_{Au}(\pi^+)/Y_{Au}(\pi^-))/(Y_D(\pi^+)/Y_D(\pi^-))$, can also be accessed, in principle, using hadron attenuation measurements. There are three potential experiments that have made, or will make such measurements in the relatively near future, and we discuss each in turn.

- HERMES measurements: HERMES has published a broad survey of hadron attenuation measurements [21], extracting the z , ν and p_t dependence of the attenuation ratio for a variety of nuclei. However, the HERMES data sample is limited to relatively low x (≈ 0.3), not large enough to access the region of significant EMC effect in the valence region.
- CLAS measurements at 5 GeV: CLAS has performed hadron attenuation measurements at an electron beam energy of 5 GeV [22]. These data do have some access

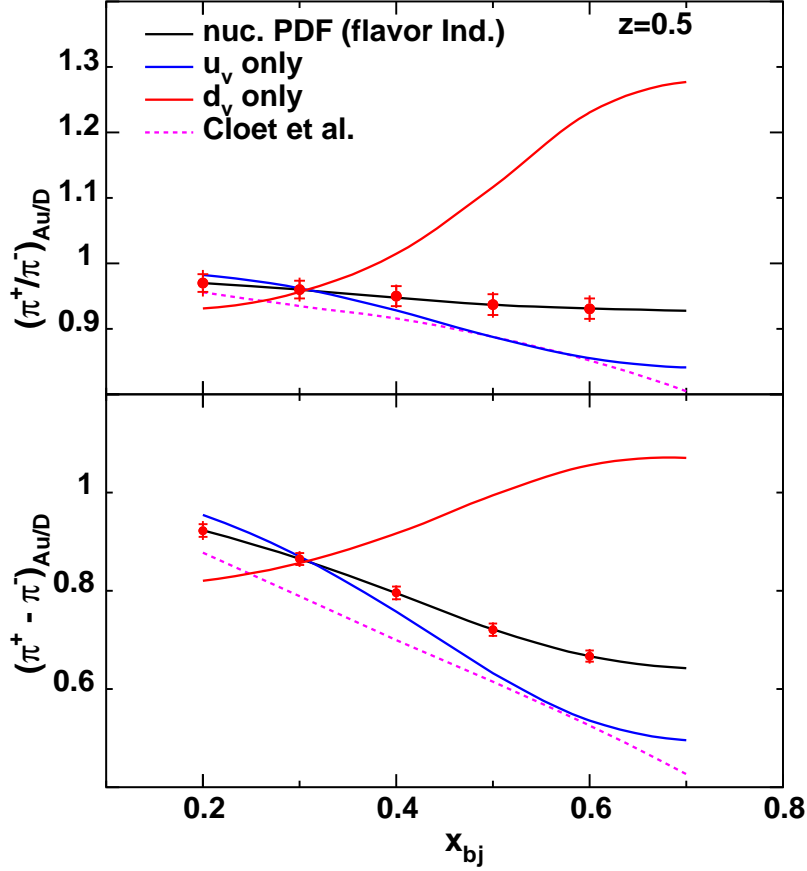


FIG. 11: Projected results for the π^+/π^- super-ratio and the difference ratio vs x at $z = 0.5$, along with calculations of the quantities described in Eqns. 9, and 11. In these calculations we show each observable under the assumption that 1) the EMC effect is the same for up and down quarks (black), 2) the EMC effect is carried entirely by the up valence quark (blue) and 3) the EMC effect is carried entirely by the down valence quark (red)). We also show the calculation of [13]. The inner error bars are statistical uncertainties and the outer error bars are the quadrature sum of statistical and systematic uncertainties.

to $x > 0.4$, the region where flavor dependence of the EMC effect may be manifest. However, the low beam energy limits access to the $x > 0.5$ where the signal may be large. Another concern is the need to cleanly identify π^- which can be problematic in CLAS. Finally, acceptance effects may play a role due to the large acceptance and open geometry of the CLAS spectrometer.

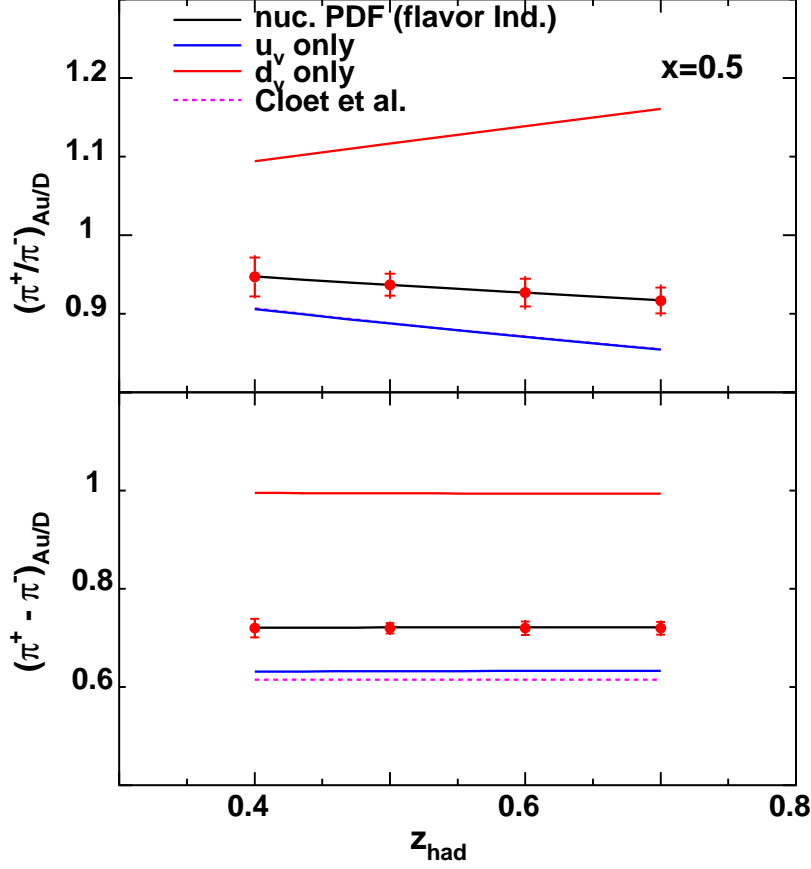


FIG. 12: Projected results for the π^+/π^- super-ratio and the difference ratio vs z at $x = 0.5$, along with calculations of the quantities described in Eqns. 9 and 11. In these calculations we show each observable under the assumption that 1) the EMC effect is the same for up and down quarks (black), 2) the EMC effect is carried entirely by the up valence quark (blue) and 3) the EMC effect is carried entirely by the down valence quark (red). We also show the calculation of [13], but at $x = 0.5$ the quark-meson coupling calculations agree exactly with the u-only calculation. The inner error bars are statistical uncertainties and the outer error bars are the quadrature sum of statistical and systematic uncertainties.

- CLAS measurements at 12 GeV: An experiment extending CLAS hadron attenuation data to higher energy has already been approved [36]. These measurements extend the kinematic coverage to larger x . However, the open geometry of the CLAS12 spectrometer may prove problematic in making precise measurements of the charged-pion

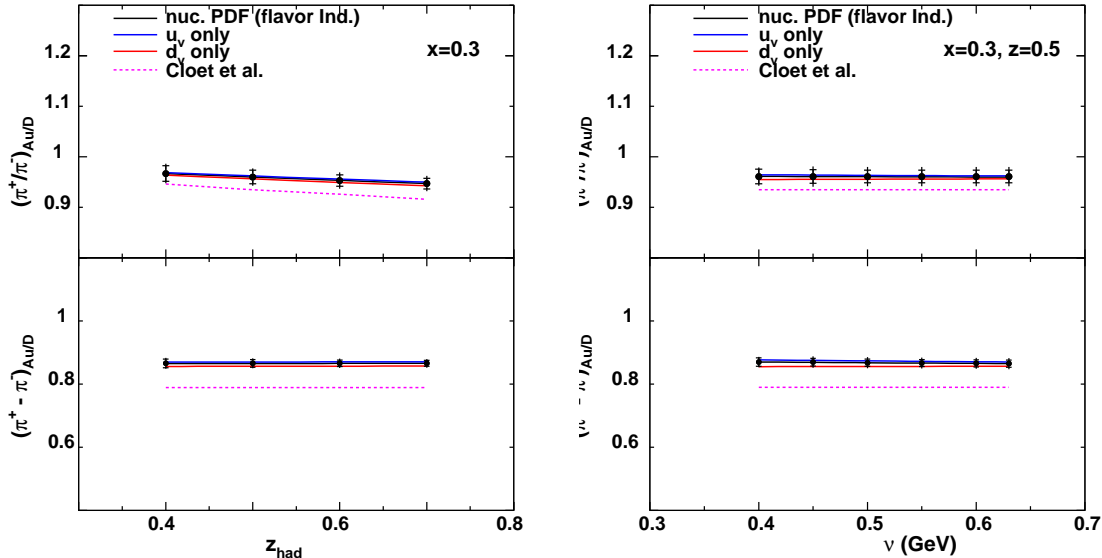


FIG. 13: Projected results for the π^+/π^- super-ratio and the difference ratio vs z (left) and vs ν (right) at $x = 0.3$, along with calculations of the quantities described in Eqns. 9 and 11. In these calculations we show each observable under the assumption that 1) the EMC effect is the same for up and down quarks (black), 2) the EMC effect is carried entirely by the up valence quark (blue) and 3) the EMC effect is carried entirely by the down valence quark (red)). Since there is no EMC effect at $x = 0.3$ they do not show any flavor dependence either. We also show the calculation of [13].

super-ratio. Magnetic focusing spectrometers present clear advantages over open geometry spectrometers when comparing positively and negatively charged particles.

To summarize, the HERMES and 6 GeV CLAS data have limited kinematic reach so are not useful for this study. The CLAS 12 GeV data will have the needed kinematic reach, but systematic uncertainties in comparing the π^+ and π^- ratios will be problematic due to the different acceptance for each charge state. Even in the optimistic scenario of a signal the size predicted using the model of Ref. [13], the potential magnitude of the effect to be measured will be only 10%. Minimizing systematic uncertainties will be crucial in gaining insight to a potential flavor dependence of the EMC effect. An experiments of this type, requiring high statistical and systematic precision in a focused kinematic regime is ideally suited to a high luminosity hall with magnetic focusing spectrometers like the HMS and SHMS.

XI. BEAM TIME REQUEST

x	z	ν	π^+ (hrs)	π^- (hrs)	π^+ (hrs)	π^- (hrs)
		(GeV)	deuterium		gold	
0.20	0.50	5.3	0.40	0.40	1.20	0.90
0.30	0.40	6.3	1.30	0.96	8.16	5.88
0.30	0.50	6.3	0.70	0.56	7.46	5.72
0.30	0.60	6.3	0.72	0.62	7.82	6.32
0.30	0.70	6.3	0.90	0.80	9.60	9.18
0.30	0.50	4.5	0.40	0.40	1.92	1.46
0.30	0.50	5.0	0.40	0.40	2.48	1.90
0.30	0.50	5.5	0.40	0.40	3.24	2.48
0.30	0.50	6.0	0.42	0.40	4.40	3.38
0.30	0.50	6.4	0.56	0.46	6.00	4.60
0.40	0.50	4.7	0.74	0.60	8.66	6.60
0.50	0.40	6.5	3.54	2.69	21.63	15.45
0.50	0.50	6.5	6.36	10.40	40.14	30.50
0.50	0.60	6.5	3.38	2.95	21.27	17.13
0.50	0.70	6.5	4.13	3.84	26.76	22.71
0.60	0.50	5.4	9.06	7.32	62.06	46.58
total			33.41	33.20	232.8	180.8
Grand total						480.2

TABLE IX: Running time for production data from gold and deuterium targets. A 10 cm deuterium and 6% r.l. gold target is assumed. Times are for 50 μA (25 μA) beam current on target for π^- (π^+) running (except for the first two kinematic points where the current is 30 μA (15 μA)). Time estimates for deuterium running assume 40,000 counts for each setting at each polarity, except at the $x = 0.5$, $z = 0.4, 0.6,$ and 0.7 . settings. 40,000 counts is assumed for all gold settings except for the $x = 0.5, 0.6$, $z = 0.5$ settings, where 20,000 counts are assumed and the $x = 0.5$, $z = 0.4, 0.6,$ and 0.7 settings where 10,000 counts are assumed.

The required production running time for this experiment is listed in Table IX. A total of 480 hours is required for data-taking on deuterium and gold targets (37 hours of this time is in common with part I of this proposal). The majority of this time (414 hours) is on the 6% gold target. This time could potentially be reduced by using a thicker target, however, previous experience in Hall C has indicated that using a target with larger than 6% radiation length presents difficulties at higher currents. For the largest x point, one could perhaps run with a large scattering chamber exit pipe at higher currents. If, for example, 80 μA were

Activity	Time
LD2 and Au data	480.2
Al. dummy data	7
LH2 data	72.1
Polarity and kinematics changes	18
Total	577.3 (24 days)

TABLE X: Total beam time request for this experiment.

available, then the last point could be completed in significantly less running time.

In addition to production data from deuterium and gold, we request ≈ 72 hours of data on liquid hydrogen to perform factorization tests at $x = 0.3$ and $x = 0.5$ using the z -scan data. Using this hydrogen data combined with the deuterium data that will be taken at those settings, we will perform tests similar to those done during Hall C experiment E00-108 (see Figure 7). We also request time for aluminum dummy data taking to subtract contributions from the liquid target cell walls.

Finally, we allocate 18 hours for various kinematic and polarity changes. At each x point, we plan to minimize systematic effects by taking data on both targets at one polarity and then changing polarity immediately and completing the setting before moving on to the next x setting. To save time, all momentum settings for the z -scan data will be taken before changing polarity. However, the resulting overhead is not terribly large given the relatively small number of kinematic settings.

Finally we note that if Part I and Part II of this proposal is approved, the combined running time would be 852 hours, or 35.5 days, 5.5 days shorter than if each were run separately due to the kinematic overlap in the deuterium data-taking.

XII. ACKNOWLEDGMENTS

The co-spokespersons would like to thank John Arrington, Antje Bruell, and Rolf Ent for helpful discussions and suggestions. They would also like to thank Ian Cloët for providing his calculation of flavor dependent EMC effect in gold.

-
- [1] J. J. Aubert *et al.* [European Muon Collaboration], Phys. Lett. B **123**, 275 (1983).
 - [2] D. F. Geesaman, K. Saito and A. W. Thomas, Ann. Rev. Nucl. Part. Sci. **45**, 337 (1995).
 - [3] P. R. Norton, Rept. Prog. Phys. **66**, 1253 (2003).
 - [4] J. Gomez *et al.*, Phys. Rev. D **49**, 4348 (1994).

- [5] K. Ackerstaff *et al.* [HERMES Collaboration], Phys. Lett. B **475**, 386 (2000) [Erratum-ibid. B **567**, 339 (2003)] [arXiv:hep-ex/9910071].
- [6] JLab Experiment 03–103, J. Arrington and D. Gaskell, spokespersons.
- [7] I. C. Cloët, W. Bentz and A. W. Thomas, Phys. Lett. B **642**, 210 (2006) [arXiv:nucl-th/0605061].
- [8] I. Sick and D. Day, Phys. Lett. B **274**, 16 (1992).
- [9] B. Lu and B. Q. Ma, Phys. Rev. C **74**, 055202 (2006) [arXiv:0705.2064 [nucl-th]].
- [10] D. M. Alde *et al.*, Phys. Rev. Lett, **64**, 2479 (1990).
- [11] J. Ashman *et al.*, Phys. Lett. **B202**, 603 (1988).
- [12] A. Airapetian *et al.* [HERMES Collaboration], Phys. Rev. D **71**, 012003 (2005) [arXiv:hep-ex/0407032].
- [13] I. C. Cloët, private communication and forthcoming publication.
- [14] M. Hirai, S. Kumano, T.-H. Nagai, Phys. Rev. C **70** 044905 (2004).
- [15] J. Binnewies, B. A. Kniehl and G. Kramer, Phys. Rev. D **52**, 4947 (1995) [arXiv:hep-ph/9503464].
- [16] P. Geiger, “Measurement of fragmentation functions at HERMES,”
- [17] A. D. Martin, R. G. Roberts, W. J. Stirling, and R. S. Thorne, Phys. Lett. **B531**, 216 (2002).
- [18] H. Mkrtchyan *et al.* Phys. Lett. B **665**, 20 (2008)
- [19] A. Airapetian *et al.* [HERMES Collaboration], Eur. Phys. J. **C21**, 599 (2001).
- [20] J. Ashman *et al.* [European Muon Collaboration], Z. Phys. C **52**, 1 (1991).
- [21] A. Airapetian *et al.* [HERMES Collaboration], Nucl. Phys. B **780**, 1 (2007) [arXiv:0704.3270 [hep-ex]].
- [22] JLab Experiment 02–104, W. Brooks, spokesperson.
- [23] T. Navasardyan *et al.* Phys. Rev. Lett. **98**, 022001, (2007).
- [24] H. L. Lai *et al.* [CTEQ Collaboration], Eur. Phys. J. C **12**, 375 (2000) [arXiv:hep-ph/9903282].
- [25] JLab Experiment 12–06–104, R. Ent and H. Mkrtchyan, spokespersons
- [26] JLab Proposal to PAC 34, “Precise Measurement of π^-/π^+ Ratios in Semi-inclusive Deep Inelastic Scattering Part I: Charge Symmetry Violating Quark Distributions”, K. Hafidi, D. Dutta, and D. Gaskell, spokespersons.
- [27] JLab Experiment 01–107, D. Dutta, R. Ent, K. Garrow, spokespersons.
- [28] B. Clasie *et al.*, Phys. Rev. Lett. **99**, 242502 (2007) [arXiv:0707.1481 [nucl-ex]].
- [29] D. E. Wiser, Ph.D. thesis, Univ. of Wisconsin (1977).
- [30] T. Sjostrand, S. Mrenna and P. Skands, JHEP **0605**, 026 (2006) [arXiv:hep-ph/0603175].
- [31] P. Liebing, Ph.D. thesis, Univ. of Hamburg (2004).
- [32] C. Hadjidakis, Ph.D. thesis, Institute de Physique Nucleaire d’Orsay (2002).
- [33] C. J. Bebek *et al.*, Phys. Rev. D **17**, 1693 (1978).
- [34] P. Brauel *et al.*, Z. Phys. C **3**, 101 (1979).

- [35] D. Drechsel, S. S. Kamalov, and L. Tiator, Nucl. Phys. **A645**, 145 (1999).
- [36] JLab Experiment 12-06-117, W. Brooks, contact person.